ISSN (Print) 1226-1750
ISSN (Online) 2233-6656
Journal of Magnetics 26(3), 277-284 (2021) https://doi.org/10.4283/JMAG.2021.26.3.277

Numerical Investigations of Radiative Flow of Viscous Fluid Through Porous Medium

Tasawar Abbas[1]*, Bilal Ahmad[1], Aaqib Majeed[2], Taseer Muhammad[3], and Muhammad Ismail[4]

[1]*Department of Mathematics, University of Wah, Wah cantt, 47000, Pakistan*
[2]*Department of Mathematics, Riphah International University, Faisalabad Campus, 38600, Pakistan*
[3]*Department of Mathematics, College of Science, King Khalid University, Abha, 61413, Saudi Arabia*
[4]*Department of Mathematics, Bacha Khan University, Charsadda, 24550, Pakistan*

(Received 29 April 2021, Received in final form 27 September 2021, Accepted 30 September 2021)

This study incorporates the numerical behavior of radiative flow of electrically conductive viscous fluid though porous medium with slip effects. The boundary is supposed to be convective during the flow. The governing nonlinear partial differential equations are transformed into its corresponding ode's with the help of suitable similarity transformations. Numerical technique is used to solve the system of ordinary differential equations. Effects of pertinent parameters on velocity and fluid temperature are plotted graphically. The velocity of fluid reduces due to opposing force offer by magnetic field whereas temperature rises.

Keywords : incompressible viscous fluid, MHD, partial slip, porous medium, viscous dissipation, thermal radiation, convective boundary

1. Introduction

Many scientists and engineers are interested to analyze the behavior of incompressible viscous flow over stretching surface due to its wide class of applications in industrial development and engineering process, for example, the production of glass fiber, drawing of wire, plastic sheet, production of paper and polymer and metal productions, and a lot of others field of industries. Crane [1] initiates the idea of investigating the flow due to linear stretching of sheet and his model is less beneficent in industrial point of view. As a result, researcher's concentrates for enhancing the idea of Crane and by examining special features of stretch rate as taken in [2].

Essentially Magnetohydrodynamics (MHD) is related to the magnetic characteristics of electrically conducting fluid. The applied magnetic field induces current which developed the fluid to get polarized. Electrolytes salt water, liquid metals, and plasma are few examples of magnetofluids. Liaquat *et al.* [3] mathematically investigated the micropolar fluid with MHD effects. Umar *et al.* [4] considered the exponentially stretched sheet to investigate the MHD behavior on Maxwell fluid. Some of relevant citations in this regard are [5-7].

Acting as an energy source, viscous dissipation alters the temperature distributions which results to affect rate of heat transfer. The worthiness of the consequence of viscous dissipation confides in whether the plate is freezed or warmed its application involves in as oil product transportation through ducts and polymer processing. Chandresarkar [8] considered the stretched flow of viscous fluid with viscous dissipation effect to analyze the flow and thermal behavior of fluid. Newtonian heating together with viscous dissipation was discussed over Casson fluid by Ahmad *et al.* [9] whereas its effects on stretching cylinder were analyze by Gayateri *et al.* [10]. Study of flow over stretched surface which is embedded in porous medium, is of fundamental attention in recent years because these phenomena are come across in various production industries and engineering processes such as brous insulation, food processing and storage, thermal insulation of buildings, geophysical systems, electrochemistry, metallurgy, the design of pebble-bed nuclear reactors, underground disposal of nuclear or nonnuclear waste, reactive polymer flows in heterogeneous porous media, electrochemical generation of elemental bromine in porous electrode systems. Hunegnaw [11] discuss the effects of incompressible fluid with MHD effects and

*Corresponding author: Tel: +92-51-9157000
Fax: +92-51-9157000, e-mail: tasawar.abbas@uow.edu.pk

considered the flow through porous medium and he gets the results of decrease in velocity of fluid. Abbas *et al.* [12] investigated the flow of dusty fluid through porous space. Nonlinear MHD flows was discussed through porous medium by Jitender [13]. Thermal radiation effects on flowing fluid plays an important part considerably at high temperature in the machinery involved astronomical field and industrial progressions functioning. During fluid flow it is considerable if there is immense temperature difference among the temperature of surface and that of an ambient temperature. Its consequences during the rotating flow of Casson fluid was analyzed by Archana *et al.* [14] in which they considered the nonlinear effects of thermal radiation over nanofluid. Harshad [15] solely considered its effects on microplar fluid in between vertical walls with heat and mass transfer. Recently Reddy and Ferdows [16] obtained the numerical solution for the flow of micropolar dusty fluid with magnetic and thermal effects across a parboiled revolution. Some recent work in this regard is given in [17-19].

The non-adherence of the fluid to a solid boundary, also known as velocity slip, is a fact which is pragmatic under definite conditions due to its applications in medical and engineering industries such as polishing of non-natural interior opening and heart valves. Doda [20] numerically investigate the velocity slip effects in compliance with MHD effects on viscous fluid and observed that in the presence of velocity slip the velocity of fluid is not same as that of boundary which inversely affects the velocity. Afterwards Mishra [21] obtained numerically the same result for the effects of velocity slips in which he considered the flow over vertical cone and obtained same results. Recently Ping *et al.* [22] discussed the second order slip effects on viscous fluid and they considered the flow over complex wavy surface. The process of heat transfer through fluid is known as convection. And the process of convective heat transfer engages in variety of engineering measures, viz. gasoline turbines, nuclear reactor plants, storage of thermal energy etc [23]. These procedures attain high temperature and the flow is considered with the convective b. conditions. As a result, a considerable figure of communication has been reported on different type of flows with different effects in addition with convective boundary condition [24-26].

According to the above literature we are able to analyze the behavior of electrically conducting viscous fluid over the stretching surface with the effects of thermal radiation and partial slip through porous medium. The system is maintained using applied convective boundary conditions. The numerical solution in the form graphs are obtained by incorporating the numerical technique RK-4 is applied with the help of MATLAB solver BVP4c.

2. Construction of Mathematical Model

We consider the steady-state 2-D convective boundary-layer flow of viscous, incompressible fluid and the fluid conducting electrically with saturated flat permeable medium caused by a linearly stretchable sheet with velocity $u_w = ax$, here "a is non-negative constant. The direction of the stretchable surface and the flow of fluid are along the sheet is a horizontal axis x-axis while normal to the sheet is a vertical axis y-axis. The flow takes place $y > 0$. Suppose that sheet is stretched linearly by considering two forces equal in magnitude and opposite in direction so that the surface of the wall is stretched, and the location of the original is remains invariant. The strength of uniform magnetic field is $B = B_0$ considered normal to the sheet (see Fig. 1). Also consider uniform surface of temperature $T_w > T_\infty$, where the T_∞ temperature of ambient fluid remain invariant.

The boundary layer partial differential continuity, momentum, and energy equations are taken the form;

$$\frac{\partial \mathcal{U}}{\partial x} + \frac{\partial \mathcal{V}}{\partial y} = 0, \tag{1}$$

$$\mathcal{U}\frac{\partial \mathcal{U}}{\partial x} + \mathcal{V}\frac{\partial \mathcal{V}}{\partial y} = \nu\frac{\partial^2 \mathcal{U}}{\partial y^2} - \frac{\sigma B_0^2}{\rho}\mathcal{U} - \frac{\nu}{K}\mathcal{U}, \tag{2}$$

$$\mathcal{U}\frac{\partial T}{\partial x} + \mathcal{V}\frac{\partial T}{\partial y} = \alpha\frac{\partial^2 T}{\partial y^2} + \frac{\mu}{\rho c_p}\left(\frac{\partial \mathcal{U}}{\partial y}\right)^2 + \frac{\sigma B_0^2}{\rho}\mathcal{U}^2 - \frac{1}{\rho c_p}\frac{\partial q_r}{\partial y}, \tag{3}$$

The appropriate slip and convective condition on the boundary is defined as follows along with the free stream conditions;

$$\begin{aligned} &y = 0,\ \mathcal{U} = \mathcal{U}_{wf} + L\frac{\partial \mathcal{U}}{\partial y},\ \ \mathcal{V} = \pm\mathcal{V}_{wf}, \\ &-k\frac{\partial T}{\partial y} = h_f\left(T_f - T_{wf}\right),\ y \to \infty,\ \mathcal{U} \to 0,\ \ T \to T_\infty \end{aligned} \tag{4}$$

Here $\mathcal{U}$ represents the velocity along the x-axis and $\mathcal{V}$

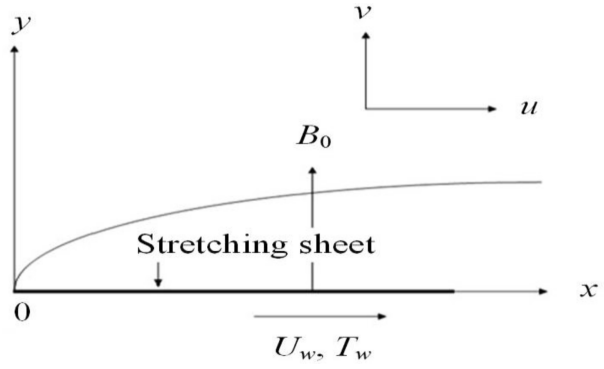

Fig. 1. Physical problem and coordinate system.

represents the velocity along the y-axis. υ denotes kinematic viscosity, σ denotes electric conductivity, ρ represents density, μ denotes dynamic viscosity, c_p represents specific heat, T denotes temperature, α represents thermal diffusivity, k represents thermal conductivity, L is the proportional constant, and T_w is the upper wall temperature of the plate.

3. Flow Analysis

Equation (11) is satisfied if we take the stream function $\Psi(x, y)$ such that

$$\mathcal{U} = \frac{\partial \Psi}{\partial y}, \quad \mathcal{V} = -\frac{\partial \Psi}{\partial x} \tag{5}$$

The Eqs. (2) and (3) are converted into the equivalent odes by considering the following similarity function:

$$\Psi(\mathrm{x},\mathrm{y}) = (\upsilon a)^{\frac{1}{2}} x f(\eta), \quad \theta(\eta) = \frac{T - T_\infty}{T_f - T_\infty}, \; \eta = \left(\frac{a}{\upsilon}\right)^{1/2} y. \tag{6}$$

Using expression (6), the above equations (2) and (3) are transformed into

$$f''' + ff'' - (f')^2 - Mf' - Pf' = 0, \tag{7}$$

$$\theta'' + \frac{3}{3+4R}\Pr(f\theta' + Ec(f'')^2 + MEc(f')^2) = 0, \tag{8}$$

The boundary equations (4) are transformed to:

$$\eta = 0, f'(\eta) = 1 + Kf''(\eta), \; f(\eta) = f_w, \; \theta'(\eta) = -\gamma\left[1 - \theta(\eta)\right],$$
$$\eta \to 0, \; f'(\eta) \to 0, \; \theta(\eta) \to 0. \tag{9}$$

Here prime represent the derivative w.r.t η.

$M_f = \sigma B_0^2/(\rho a)_f$, is a magnetic parameter, $Ec = u_w^2/(c_p(T_f - T_\infty))$ is Eckert number, $Pr = \mu_f c_p/k_f$ is Prandtl number, $K = L\left(\frac{a}{\upsilon}\right)^{1/2}$ is slip parameter, $\gamma = h_f\left(\frac{\upsilon}{a}\right)^{1/2}/k$ show that the conjugate parameter for convective boundary condition, $P = \frac{\upsilon}{k^* a}$, is the permeability parameter, $R = \frac{4\sigma_f T_\infty}{(k^* k)_f}$, is the radiation parameter, and $q_r = \frac{-4\sigma^* \partial T^4}{3k^* \partial y}$ is the radiative heat flux when $\gamma = 0$ an insulated wall is present, and when $\gamma \to \infty$ the wall temperature is prescribed. $f_w = \mp \frac{v_w}{\sqrt{a\upsilon}}$, represents the parameter for suction/injection.

The skin friction coefficient or wall shear stress is an important dimensionless parameter in boundary-layer flows. It specifies the fraction of the local dynamic pressure, that is felt as shear stress on the surface and therefore it is the resistive force exerted by surface during the flow. Furthermore the local Nusselt number is another important dimensionless number in engineering point of view as it is the phenomena of heat transfer due to pure conduction and its significance enables to design more efficient thermal engineering systems. Based on these important facts the corresponding value of shear stress C_f and heat flux Nu_x at wall is formulated for this model as

$$C_f = \frac{\tau_{wf}}{\rho u_{wf}{}^2}, \quad Nu_x = \frac{q_{wf} x}{k_f(T_w - T_\infty)}, \tag{10}$$

here τ_{wf} is represent the shear stress and heat flux of the wall of the fluid is denoted by q_{wf} and define by

$$\tau_{wf} = \mu_f\left(\frac{\partial u}{\partial y}\right)_{y=0}, \; q_{wf} = -k_f\left(\frac{\partial T}{\partial y}\right)_{y=0}. \tag{11}$$

Using equations (11) the expression (10) becomes

$$1/2C_f(\mathrm{Re}_x)^{1/2} = f''(0), \; Nu_x(\mathrm{Re}_x)^{-1/2} = -\theta'(0). \tag{12}$$

where $\mathrm{Re} = \frac{u_w x}{\nu}$ is Reynolds Number.

4. Numerical Procedure

The transformed constitutive equation of momentum and energy transport are coupled and highly non-linear which is very difficult to obtain a closed-form solution, so we will try to solve these equations numerically by employing the bvp4c procedure with the help of the Matlab software package. The three-stage LobattoIIIa formula is created in *bvp4c* with the help of a finite difference code. Afterward, stability analysis is performed using the *bvp4c* solver function. According to Shampine *et al.* [33] "this collocation formula and the collocation polynomial provide a C1 continuous solution that is fourth-order accurate uniformly in [a, b]. Mesh selection and error control are based on the residual of the continuous solution". Further, the tolerance of the relative error is fixed at 10^{-5}. The suitable mesh determination is created and returned in the field sol.x. The *bvp4c* returns the solution, called sol.y., as a construction. In any case, values of the solution are gotten from the array named sol.y, relating to the field sol.x. The general procedure of this method, along with stability analysis, is presented in Figure (Flow chart)

In the bvp4c procedure, we select appropriate limited values of $\eta \to \infty$, say $\eta_\infty = 7$. In this scheme, the finite difference method is employed which gives fourth-order accuracy. For this first, we convert the equation (7) and

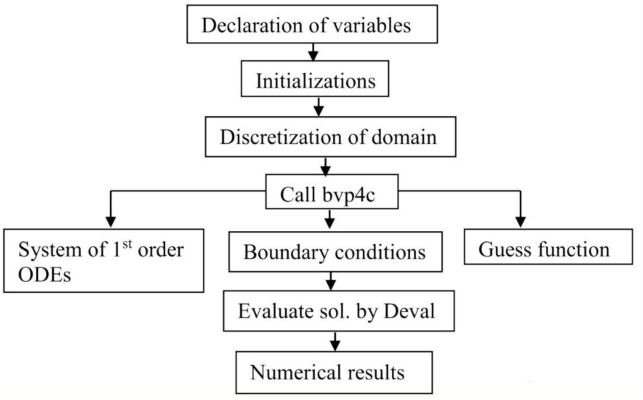

Flow Chart

(8) into equivalent linear ordinary differential equations as:

$$y(1) = f$$
$$y(1)' = y(2) = f'$$
$$y(2)' = y(3) = f''$$
$$y(3)' = f''' = -y(1)y(3) + y(2)^2 + My(2) + Py(2)$$
$$y(4) = \theta,$$
$$y(4)' = y(5) = \theta',$$
$$y(5)' = \theta'' = \frac{-3Pr}{3+4R}(y(1)y(5) + Ecy(3)^2 + MEcy(2)^2), \quad (13)$$

and the boundary conditions are

$$y_a(1) = f_w,\ \ y_a(2) = 1 + Ky(3),\ y_b(2),$$
$$y_a(5) = -\gamma\big(1 - y_a(4)\big),\ y_b(4). \quad (14)$$

A suitable step size $\delta = 0.001$ is selected for the entire numerical computation work. A possible convergence limit has been adopted as 10^{-6}. Furthermore, the boundary conditions given in (9) value at infinity is chosen as $\eta(\infty) = 4$; after selecting the appropriate value for $\eta(\infty)$, all numerical solutions converge to it and are satisfied correctly. Finally, residual error analysis has been evaluated.

5. Results and Discussions

In this section, the mathematical calculation has been done by using the numerical procedure as defined earlier for numerous convergence flow parameters like Prandtl, no (*Pr*), Eckert no (*Ec*), convective parameter to find the $f'(\eta)$ $\theta(\eta)$ and profiles. Also, Tables 1-2 is representing the $1/2C_f(\mathrm{Re}_x)^{1/2}$ (skin friction coefficient) and $Nu_x(\mathrm{Re}_x)^{-1/2}$ (Nusselt number) against the variation of different parameters. Table 3 portrays the comparison of $Nu_x(\mathrm{Re}_x)^{-1/2}$ (Nusselt number) with those obtained by previous researchers show superb accuracy. The numeric values of the parameter throughout the problem are taken as $K = 0.20$, $R = 0.20$, $f_w = 0.20$, $P = 0.20$, $\gamma = 0.20$

Table 1. Values of $1/2C_f(\mathrm{Re}_x)^{1/2}$ under slip factor *K*.

M	*K*	Present result	Anderson [2]	Wang [15]	Sahoo & do [4]
0	0	1.2000	1.0000	1.000	1.001154
0	1	0.4873	0.4302	0.430	0.428450
0	2	0.3162	0.2840	0.284	0.282893
0	5	0.1579	0.1448	0.145	0.144430

Table 2. Results $-\theta'(0)$ for numerous results of γ when $M = P = K = Ec = R = f_w = 0.2$ and $Pr = 1.0$.

γ	Present Result	Aziz [7]	Ishak [3]	Rahman [14]
0.0	0.0000	0.0373	0.0368	0.0369
0.1	0.0736	0.0594	0.0583	0.0584
0.2	0.1267	0.0848	0.0823	0.0824
0.4	0.1983	0.1076	0.1037	0.1038
0.6	0.2444	0.1128	0.1135	0.1136
0.8	0.2765	0.1243	0.1191	0.1193
1.0	0.3001	0.1283	0.1228	0.1229
2.0	0.3620	0.1430	0.1362	0.1364
5.0	0.4131	0.1450	0.1380	0.1382
20	0.4445	0.1461	0.1390	0.1392

Table 3. Results of $-\theta'(0)$ for several results of *Ec* and *Pr* with $M = P = K = \gamma = R = f_w = 0.2$.

Pr	*Ec*	$-\theta'(0)$
0.72	0.2	0.1188
1.00	0.2	0.1267
2.00	0.2	0.1407
0.72	0.0	0.1342
0.72	0.25	0.1150
0.72	0.50	0.0958

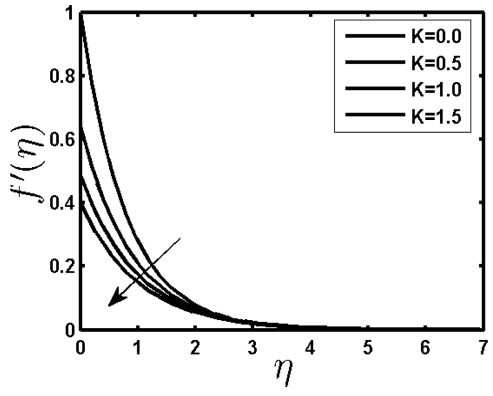

Fig. 2. Effect of *K* on $f'(\eta)$.

$Pr = 1.00$, $M = 0.20$, $Ec = 0.20$ and Fig. 2 displays the influence of the slip factor (*K*) on $f'(\eta)$ the field. From the figure, it is detected that $f'(\eta)$ of fluid is decreasing by the rising slip factor (*K*). Physically, slip effect para-

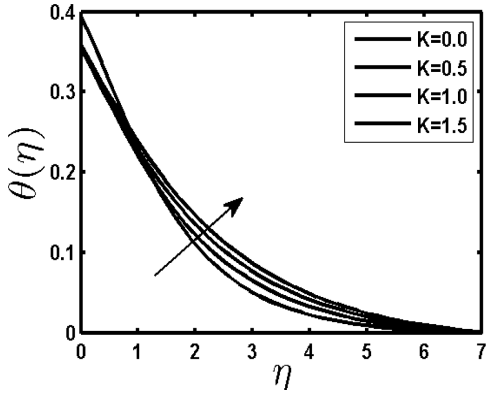

Fig. 3. Effect of K on $\theta(\eta)$.

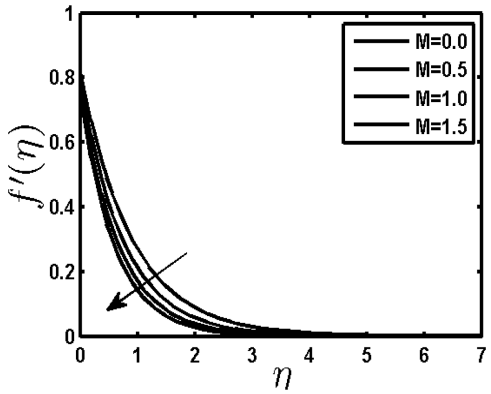

Fig. 4. Effect of M on $f'(\eta)$.

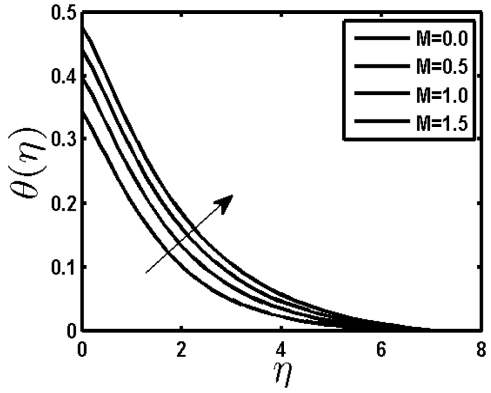

Fig. 5. Effect of M on $\theta(\eta)$.

meter enhances the factors offering opposition of fluid motion, which diminishes the fluid flow field and momentum boundary layer thickness. Fig. 3 shows that with the rise in slip factor (K), the temperature at a point initially decreases for small values of η and after a definite point it increases with (K). Fig. 4 illustrates the impact of magnetic factor (M) on $f'(\eta)$ profiles. From the figure, it is detected that velocity profile of fluid reduced by rising magnetic parameter (M). This is for the fact that strengthening the magnetic fluid causes to

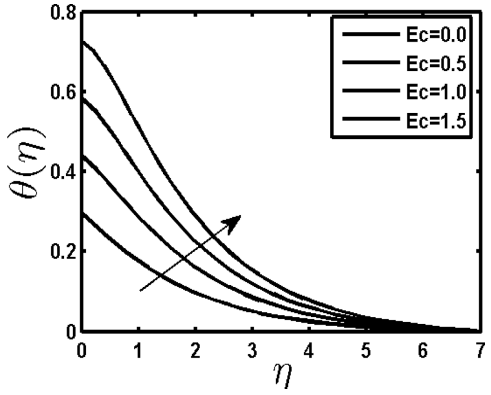

Fig. 6. Effect of Ec on $\theta(\eta)$.

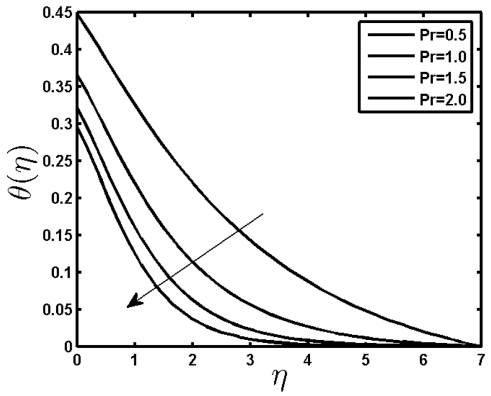

Fig. 7. Effect of Pr on $\theta(\eta)$.

develop the opposed strength to the flow is named the Lorentz force. This force works opposite to the flow which yields more resistance to the transport sensations. Fig. 6 displays the impression of the Eckert parameter (Ec) on $\theta(\eta)$. From the figure, it is detected that fluid temperature enhances by rising Eckert parameter (Ec). This is because for greater values of the Eckert number there are significant peers of heat due to viscous dissipation near the sheet. Therefore viscous dissipation in a flow-through porous surface is useful for gaining the temperature. We can tell that raising the Eckert number (Ec) rises $\theta(\eta)$ as the heat energy is set down in the fluid due to the frictional heating. Fig. 7 displays the impact of the Prandtl number on $\theta(\eta)$. The thermal boundary layer thickness develops the same as the velocity boundary layer when a coolant is flowing at temperature T over a cladding or surface at different temperature T_s (Figure below). This boundary develops until meeting the criteria at which: $(T - T_s)/(T_\infty - T_s) = 0.99$. The thickness of velocity and thermal boundary layers can be described from the Prandtl number values. For example, for liquid metals (low Prandtl number values), the molecular diffusivity of heat is higher than molecular diffusivity of

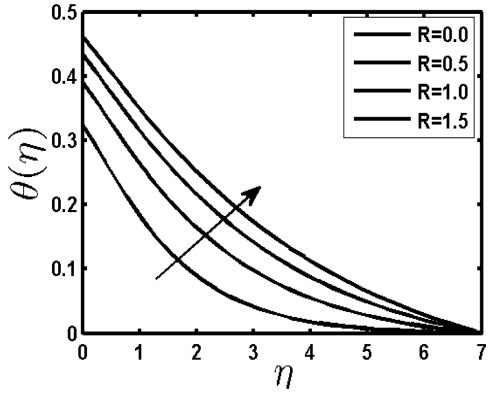

Fig. 8. Effect of R on $\theta(\eta)$.

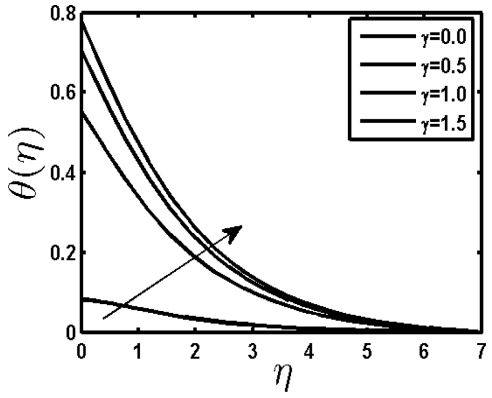

Fig. 9. Effect of γ on $\theta(\eta)$.

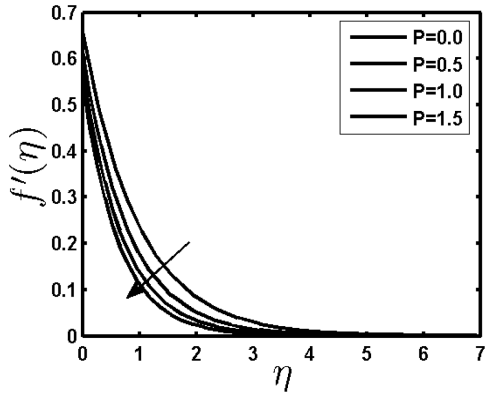

Fig. 10. Effect of P on $f'(\eta)$.

momentum, which leads to higher thermal boundary layer thickness than the velocity boundary layer. From the figure, it is detected that $\theta(\eta)$ fluid is decreased by the rising Prandtl parameter (Pr). Fluids with lesser Prandtl number will take greater thermal conductivities (α) therefore heat can diffuse from the surface quicker than for greater (Pr). Hence thermal boundary layer thickness decreases with the rise of the Prandtl number. Fig. 8 displays the result of the radiation factor (R) on $\theta(\eta)$ profiles. From the figure, it is observed that temperature

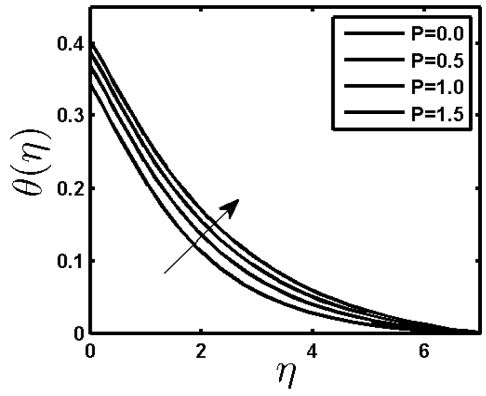

Fig. 11. Effect of P on $\theta(\eta)$.

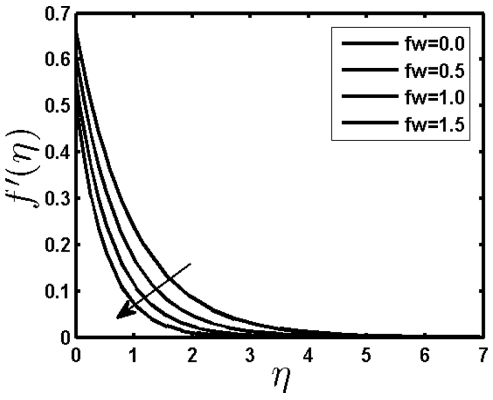

Fig. 12. Effect of f_w on $f'(\eta)$.

of fluid enhances by intensifyingthe values of radiation factor (R). This is because for large values of (R) telling of higher quantity of radiative heat energy being transferred into the system, producing an increment in $\theta(\eta)$. Fig. 9 displays the impacts of a convective factor γ on the $\theta(\eta)$ sketch. It is found that the rise of γ the $\theta(\eta)$ fluid also rises. Physically it distinguishes the proportion of interior conduction protection from outside convective obstruction. Higher values of convective parameter inversely affect the thermal resistance of the surface and because of this the convective heat transfer to the viscous fluid increases. Fig. 10 displays the $f'(\eta)$ sketch for several results of permeability factor (P). It can be realized that the velocity profile falls by the rise of the permeability factor (P). Increase in permeability of porous medium offers more resistance to the flow which results in form of decrease in velocity. On the other hand the temperature of fluid increases due to increase resistance in case of rising porosity parmetr values as shown in Fig. 11. Fig. 12 and 13 show that the impacts of suction/injection factor f_w on $f'(\eta)$ and $\theta(\eta)$. From figures, it is detected that $f'(\eta)$ and $\theta(\eta)$ of fluid falls by rising suction/injection factor (f_w). This is because of

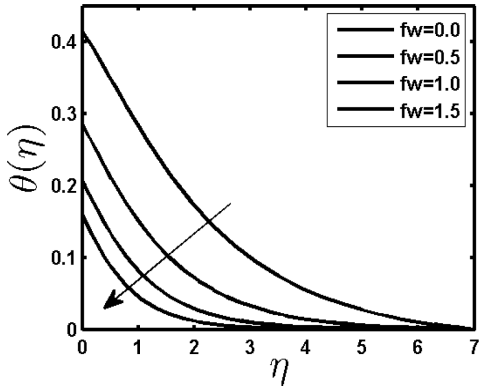

Fig. 13. Effect of f_w on $\theta(\eta)$.

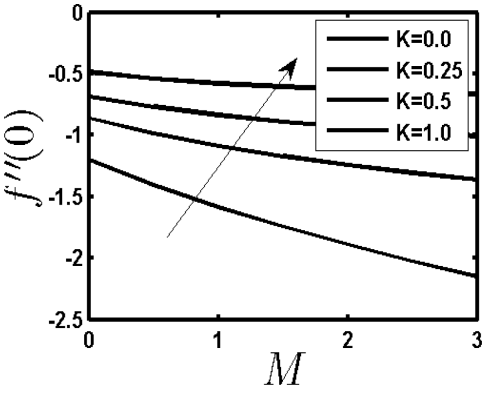

Fig. 14. Effect of K on $f''(0)$.

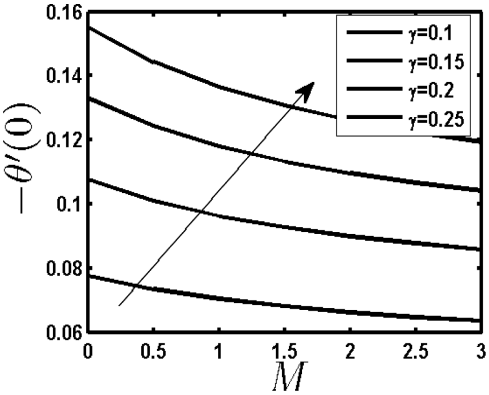

Fig. 15. Effect of γ on $-\theta'(0)$.

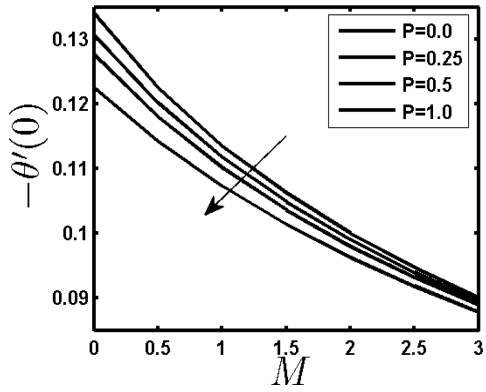

Fig. 16. Effect of P on $-\theta'(0)$.

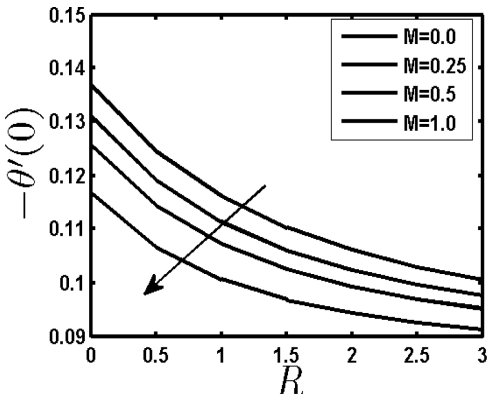

Fig. 17. Effect of M on $-\theta'(0)$.

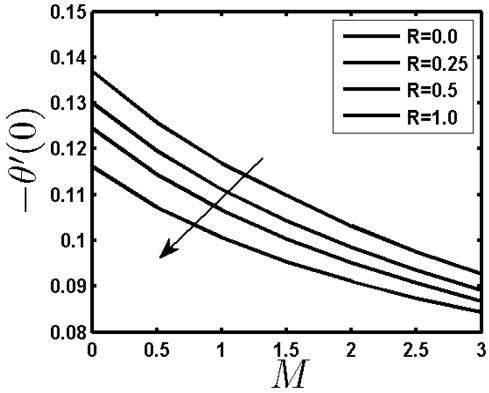

Fig. 18. Effect of R on $-\theta'(0)$.

fact that the injection allows fluids to enter into the system and hence the magnetic parameter effectively raises the thermal boundary layer thickness in the injection case. Besides the imposed injection causes the reduction of boundary layers and also leads to fast cooling of the sheet.

The physical quantity such as $1/2C_f(\mathrm{Re}_x)^{1/2} = f''(0)$ (skin friction coefficient) with magnetic factor (M) for numerous results of slip factor (K) and permeability parameter (P) is offered in Fig. 14 and 19. It is shown that $f''(0)$ rises with rising of (K) and decreases with increasing the value of (P). Fig. 15 shows that $-\theta'(0)$ rise with swelling values of γ. Fig. 16 shows that $-\theta'(0)$ fall with raising the values of permeability factor. Fig. 17 and 18 illustrate the variation of $-\theta'(0)$ for the different value of (M)(R) and. Thus for small values (R) $-\theta'(0)$ the sheet gives fluctuating nature with R but for large values of (M), $-\theta'(0)$ decrease. Table 3 offers the values $-\theta'(0)$ for various results of (Pr)(Ec) and. It is observed that $-\theta'(0)$ rises with raising the values of (Pr), while it falls

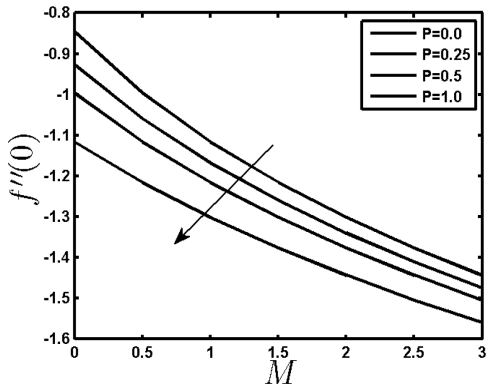

Fig. 19. Effect of P on $f''(0)$.

with increase of (Ec) .

6. Conclusion

A numerical study is performed for the incompressible boundary layer flow and heat transfer analysis towards a stretchable surface. By applying the similarity approach to transform the PDE's into ODE's, which are then solved with the help of MATLAB. Also the impact of different physical parameters is inspected on the flow field through graphs and tables. The comparison of the present results is also made with the previous ones. In the light of existing results, the following key points are summarized as:

- Temperature profile shows increasing impact by rising magnetic.
- Impact of slip parameter decreases the velocity profile while it increases the temperature profile.
- Temperature profile reduces by increasing the Prandtl number.
- For large value of radiation gives the higher quantity of radiative heat energy being transferred into the system, which produces the increment in temperature field.

References

[1] L. J. Crane, J. Appl. Math. Phy. (ZAMP) **21**, 645 (1970).
[2] M. Turkyilmazoglu, Int. J. Nonlinear Mechan. **83**, 59 (2016).
[3] L. A. Lund, Z. Omar, I. Khan, Heliyon **5**, (2019).
[4] U. Farooq, D. Lu, S. Munir, M. Ramzan, M. Suleman and S. Hussain, Sci. Rep. **9**, (2019).
[8] C. Muthukumaran and K. Bathrinathan, Symmetry **12**, (2020).
[9] K. Ahmad, Z. Wahid, and Z. Hanouf, J. Phys.: Conf. Ser. **1127**, 012028 (2019).
[10] M. Gayatri, K. J. Reddy, and M. J. Babu, SN Applied Sciences **2**, 494 (2020).
[12] Z. Abbas, J. Hasnain, and M. Sajid, J. Enging Thermophs. **28**, 84 (2019).
[13] J. Singh, U. S. Mahabaleshwar, and G. Bognár, Sci. Rep. **9**, 18484 (2019).
[14] M. Archana, B. J. Gireesha, B. C. Prasannakumara, and R. S. R. Gorla, J. Nonlinear Eng. 1092529093 (2017).
[15] H. R. Patel, Int. J. Ambient Energy (2019) 1281-1296.
[16] M. Gnaneswara Reddy and M. Ferdows, J. Therm. Anal. Calorim. **143**, 3699 (2021).
[17] S. B. Kejela, M. Daba, and A. Girum, J. Math. 5590657 (2021) pp 1-15.
[18] M. Rooman, M. A. Jan, Z. Shah, P. Kumam, and A. Alshehri, Sci. Rep. 11 (2021).
[19] Y. Q. Song, S. A. Khan, M. Imran, H. Waqas, S. Khan, M. Khan, S. Qayyum, and Yu-M. Chu, Alex. Eng. J. **60**, 4607 (2021).
[20] D. Ramya, R. S. Raju, J. A. Rao, and A. J. Chamkha, Propuls. Power Res. **7**, 182 (2018).
[21] A. Mishra, K. Pandey, and M. Kumar, Nano. Sci. Technol.: An Int. J. **10**, 169 (2019).
[22] P. Y. Xiong, K. Javid, M. Raza, S. U. Khan, M. I. Khan, and Y. M. Chu, Commun. Theor. Phys. **73**, (2021).
[23] S. S. P. M. Isa, N. Md. Arifin, R. Nazar, N. Bachok, and F. Md. Ali, IOP Conf. Series: Journal of Physics: Conf. Series 949 (2017).
[24] A. Neeraja, R. L. V. R. Devi, B. Devika, and V. N. Radhika, M. K. Murthy, Results Eng. 4 (2019).
[25] K. A. Maleque, Int. J. Aerosp. Eng. 7486971 (2020) pp 1-9.
[26] S. I. Opadiran and S. S. Okoya, Heliyon, 7 (2021).
[27] H. I. Andersson, Acta Mech. **158**, 121 (2002).
[28] C. Y. Wang, Chem. Eng. Sci. 57 (2002).
[29] B. Sahoo and Y. Do, Int. Commun. Heat Mass Transf. 37 (2010).
[30] T. Aziz, F. M. Mahomed, A. Shahzad, and R. Ali, J. Mech. **30**, (2017).
[31] A. Ishak, Appl. Math. Comput. **217**, (2010).
[32] M. M. Rahman, Meccanica 46 (2011).
[33] L. F. Shampine, I. Gladwell, and S. Thompson, Cambridge Unv. Press (2003).